Soft x-ray photoemission of clean and sulfur-covered polar ZnO surfaces: A view of the stabilization of polar oxide surfaces

Jayeeta Lahiri,[1] Sanjaya Senanayake,[2] and Matthias Batzill[1]
[1]*Department of Physics, University of South Florida, Tampa, Florida 33620, USA*
[2]*Chemical Sciences Division, Oak Ridge National Laboratory, Oak Ridge, Tennessee 37830, USA*
(Received 4 June 2008; revised manuscript received 24 August 2008; published 10 October 2008)

The two polar surfaces of ZnO were investigated by soft x-ray photoemission spectroscopy. Surface components due to variation in the Madelung energy were identified in photoemission core-level spectra. Sulfur adsorption was used to passivate the surfaces in order to enable separation of the bulk from the surface components. For the ZnO(0001)-Zn surface the observed photoemission peaks were consistent with a Zn-deficient surface, exhibiting a high density of O-terminated step edges. The ZnO(000–1)-O surface is very reactive toward hydrogen adsorption and only above 650 K a hydrogen free surface was observed. For hydrogen-free and small hydrogen coverage an electrostatic shift of the Fermi-level toward the band-gap center was observed. This indicates an incomplete compensation of the internal electrostatic potential by surface oxygen vacancies or charged adsorbates. Coadsorption of sulfur lowered the desorption temperature for hydrogen indicating the possibility to tune the chemical properties of these polar surfaces by dopants.

DOI: 10.1103/PhysRevB.78.155414 PACS number(s): 79.60.−i, 68.35.B−, 68.47.Gh, 82.45.Jn

I. INTRODUCTION

Photoemission core-level peak positions contain information about the physical and chemical environment of the emitting atoms. However, the origin of peak shifts is not always easily determined since different contributions are often present at the same time and peak deconvolution can be challenging.[1] Here we exploit surface effects in core-level photoemission lines in order to obtain information about the surface properties of the polar ZnO surfaces. The low kinetic energy of the photoemitted electrons in soft–x-ray photoemission spectroscopy (SXPS) assures a high surface sensitivity and thus enables us to measure properties of the topmost surface layers. Thus the aim of this paper is to determine surface effects in the core-level photoemission spectra and use this information to understand the stabilization mechanism of the polar surfaces of ZnO.

Polar surfaces, i.e., bulk truncations of (partially) ionic materials with a dipole moment in the repeat unit would have a diverging electrostatic potential if the surfaces remained in their bulk truncation and charge states.[2] To stabilize these surfaces, charges are transferred from one polar surface to the other.[3,4] In the absence of any compositional and structural surface variations, the surface electronic structure will change. This is schematically illustrated in Fig. 1. The electrostatic potential due to the internal dipole moments causes a shift of the electronic levels relative to the Fermi level in opposite directions at the two polar surfaces as shown in Fig. 1(b). In this simplified schematic the potential due to the internal dipole causes a shift of the energy levels relative to the Fermi level until the valence band is depleted on one side and the conduction band filled on the opposite side. Conceptually this would result in a charge transfer from one side to the other and consequently a potential that counteracts the potential due to the lattice dipole. Thus even if the bulk electronic structure were maintained, this charge transfer would prevent a divergence of the electrostatic potential due to the lattice dipole. Therefore, the electronic degrees of freedom always prevent the divergence of the surface energy of polar surfaces. Such a charge-transfer mechanism is, however, still associated with significant energy cost and polar surfaces may find alternative ways to balance the internal dipole by means that are thermodynamically favored. Stabilization of polar surfaces is most commonly accomplished by surface reconstructions that alter the surface composition in such a way that the altered ion concentration compensates the internal dipole moments. Adsorption of impurities also plays often an important role in stabilizing polar surfaces. To complicate the issue a combination of these "fundamental" stabilization mechanisms can result in the necessary stabilization. Furthermore, the stabilization mechanism for the two opposing polar surfaces can be different.

For the two polar ZnO surfaces, shown in Fig. 1(a), different stabilization mechanisms have been proposed. For the ZnO(0001)-Zn surface the probable stabilization of the clean surface in ultrahigh vacuum is by removal of $\sim 1/4$ ML of Zn atoms from the surface in a nonperiodic manner. This is achieved by formation of high density of triangular shaped pits and ad islands that exhibit step edges that are O-terminated as shown in Fig. 2.[5,6] For the ZnO(000–1)-O surface the stabilization mechanism is not fully explained yet and all of the above mentioned stabilization mechanisms have been invoked in the past. Wöll and co-workers observed a 1×3 surface reconstruction for a clean surface, which they interpreted as an ordered array of O-vacancies with 1/3 oxygen atoms missing.[7] This structure does, however, not entirely satisfy the electrostatic stabilization criteria (which requires $\frac{1}{4}$ ML of missing oxygen) and density-functional theory calculations have shown that it is not a stable surface structure.[8,9] Nevertheless, the observed superstructure is an indication for structural surface reconstruction. On the other hand, Wöll and co-workers proclaimed that surfaces that did not exhibit the 1×3 reconstruction were hydrogen terminated. This observation was disputed by others who claimed that a 1×1 hydrogen-free surface can be prepared.[10] *Ab initio* thermodynamics calculations for vary-

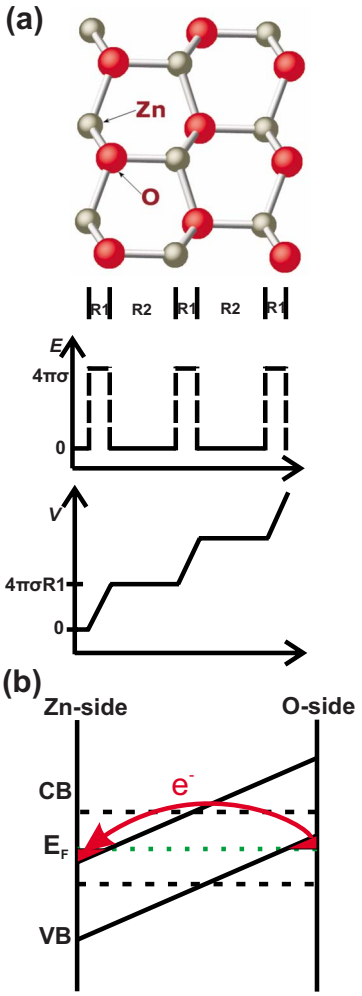

FIG. 1. (Color online) (a) Spatial variation in the electric field $\boldsymbol{E}$ and of the electrostatic potential $\boldsymbol{V}$ in a sample cut along a polar direction where $\boldsymbol{\sigma}$ is the charge density on the planes (adapted from Ref 3). (b) Schematic of surface metallization: The conduction and valence-band edges (CB and VB) are shown relative to the Fermi level E_F in a crystal terminated by two polar surfaces. The potential due to the mechanism shown in (a), causes the electronic bands to shift relative to the Fermi-level. Once the CB and VB intersect the Fermi-level charges are redistributed from one side to the other. This results in a potential opposing a divergence of the surface potential due to the lattice dipole. Since in this scenario the Fermi level is within allowed electronic states at the surface this mechanism is referred to as "metallization" of the surface.

ing hydrogen and oxygen chemical potentials, allowed a construction of a phase diagram.[11] This diagram showed that a phase with a $\frac{1}{4}$ oxygen atoms missing is the stable phase under O and H poor conditions. However, it was doubted that these conditions can be achieved. Under realistic conditions hydrogen termination was predicted with different stable phases with hydrogen coverage of $\frac{1}{2}$, $\frac{1}{3}$, and $\frac{1}{4}$ ML. Those phases have, however, not been experimentally confirmed and thus there still exists controversy about the surface properties of the polar ZnO surfaces.

Here we use photoemission to study the two polar surfaces. Core-level photoemission lines contain information on the surface properties. Chemical shifts, i.e., shifts due to the

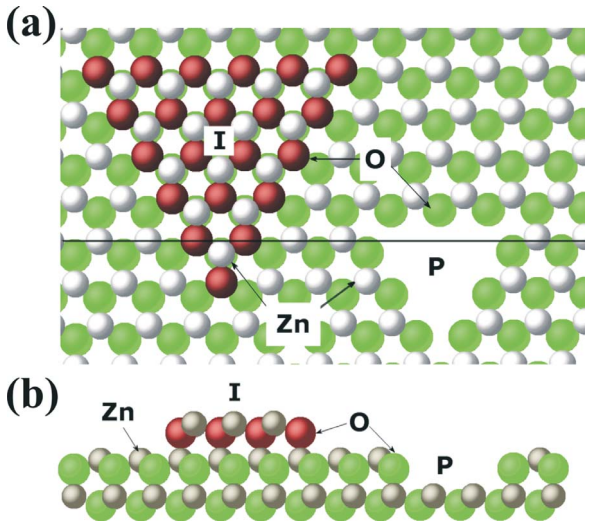

FIG. 2. (Color online) Top view of the ZnO(0001)-Zn surface showing triangular pits(p) and islands(i). The step edges exhibit threefold coordinated oxygen atoms compared to the fourfold coordination on the terraces. The cross section indicated in (a) is shown in (b).

charge state of the photoemitting element, are most commonly exploited to obtain information. In addition on ionic materials changes in the Madelung energy causes shifts in the core-level position of the surface atoms compared to the bulk. This shift is usually restricted to the atoms in the surface layer as the Madelung energy quickly approaches the bulk value. Furthermore since the Madelung energy depends on the local coordination of the surface atoms different shifts may be expected for surface atoms in different constellations, i.e., for example, atoms at step edges compared to terraces. In principle a deconvolution of the core-level peaks into its different components should enable us to determine the concentration for these different sites.

For surfaces with unknown surface structure and composition surface core-level shifts may be used to obtain a better understanding of the surface. This may apply for the ZnO(000–1)-O surfaces. The effects of the Madelung energy on surface core-level shifts for ZnO has been estimated some time ago, but to our knowledge this is the first time that the surface shift in ZnO core levels has been measured.[12]

Upon appropriate calibration of the photon energy and the analyzer work function, photoemission spectroscopy gives the binding energy (BE) of electronic states relative to the Fermi level of the material. Thus core-level and valence-band states can be referenced relative to the Fermi level. In semiconductors shifts in electronic states relative to the Fermi-level occur due to electrostatic band bending induced by surface charges and dipole moments. Photoemission is a commonly used technique to measure this electrostatic band bending at interfaces by monitoring binding energies of electronic states.[13] Here we use this capacity of photoemission spectroscopy to compare the Fermi-level position for the two polar surfaces to identify a relative shift of the Fermi level for the two surfaces. Such a shift is expected if the internal dipole moment is not compensated by surface reconstructions or impurities as it is illustrated in Fig. 1(b). Further-

more, core level and valence-band shifts are utilized to measure the band bending induced by the formation of a surface sulfide layer.[14]

II. EXPERIMENTAL PROCEDURES

The experiments were performed at the U12a soft x-ray beamline at the National Synchrotron Light Source at Brookhaven National Laboratory. The base pressure in the UHV chamber was in the low 10^{-10} Torr range. A two side polished 0.5 mm thick ZnO single crystal with polar surface orientation from Scientific Production Co. Goodwill was used. The crystal was broken in half and both halves were mounted on a 0.5 mm thick tantalum plate. One half exposed the Zn terminated side and the other half exposed the O-terminated side. Thus both orientations could be measured under identical conditions and thus enabling a direct comparison of binding energies for the two surfaces. In order to change from one sample to the other only a translation of the manipulator was necessary. The samples were heated by means of Ta wires that were spot welded to the sample mounting plate. These wires were heated by a direct current. The temperature of the Ta-support plate was measured with a thermocouple and this is taken as the reported sample temperature.

The ZnO samples were cleaned by cycles of 1 keV Ar^+ ion sputtering and annealing to 900 K. No surface contaminations were observed in SXPS survey scans. In order to differentiate between bulk and surface state the surface was passivated with (sub) monolayer sulfide. This was accomplished by backfilling of the UHV chamber with H_2S with the sample at 600 K. The H_2S exposure was measured with an ion gauge. The photoemission spectra reported here, if not mentioned otherwise, were acquired at a sample temperature of 600 K. This served several purposes: (i) to allow dissociative adsorption of H_2S and formation of sulfide overlayer, without the need to raise sample temperature during exposure, (ii) to increase the sample conductivity and thus avoid charging effects (cooling below room temperature caused charging induced peak shifts), and most importantly (iii) to keep the surface clean from adsorbates. In particular, the O side quickly accumulated hydrogen as evident in a pronounced OH component in the O-1*s* core level if the sample temperature was lowered.

The XPS data were collected using a VSW 125 hemispherical analyzer with the sample oriented such that the photon incident angle was 35° and electron emission angle was 30° relative to the surface normal. The instrumental resolution was ca. 0.5 eV. The photon energies were calibrated by using the energy separation of core-level peaks excited by first and second-order light. In order to provide absolute numbers for the binding energy relative to the Fermi level of ZnO we calibrated the analyzer work function by measuring the Fermi edge on the tantalum-metal sample holder. Photon energies of $h\nu=630$ eV and $h\nu=150$ eV were chosen for the O-1*s* and Zn-3*d* peaks, respectively. This resulted in kinetic energies of 116.6 and 133.3 eV and thus a similar surface sensitivity.

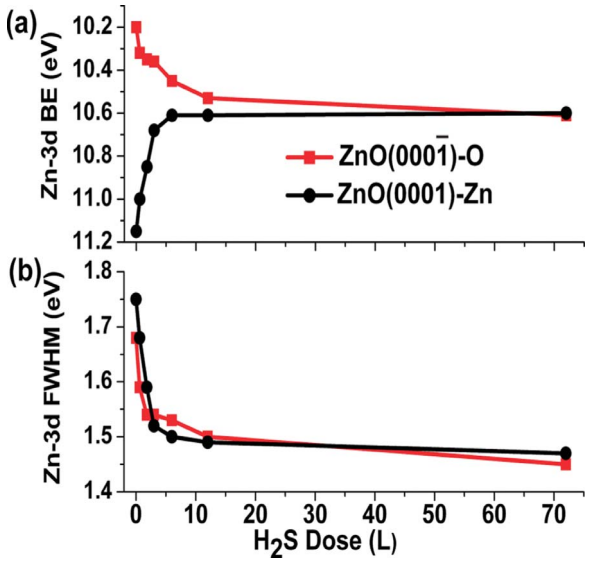

FIG. 3. (Color online) The change in the binding energy due to band bending (a) and the FWHM (b) of the Zn-3*d* peak with increasing H_2S exposure for both the Zn-terminated and the O-terminated surfaces are shown, respectively.

III. RESULTS

For the ZnO(0001)-Zn surface, the Zn-3*d*, O-1*s*, S-2*p* core levels and the valence band were monitored for increasing H_2S exposure at 600 K. At this temperature a sulfide ad layer is forming that also induces an upward surface band bending, i.e., a shift of the core levels to lower binding energy. This shift of the binding energy of the Zn-3*d* core level as a function of H_2S exposure is shown in Fig. 3(a). The resulting surface band alignment between surface sulfide and the substrate has been reported previously in Ref 14. At the same time the full width at half maximum (FWHM) is becoming narrower with increasing surface sulfur coverage [Fig. 3(b)]. A similar peak narrowing is observed for the O-1*s* peak. This indicates that there is more than one component to describe the peak shape of the clean surface. Figures 4 and 5 show the O-1*s* and Zn-3*d* peaks for different H_2S exposures, respectively.

For the ZnO(000–1)-O surface, a similar peak narrowing of the clean surface is observed for both the Zn-3*d* [see Fig. 3(b)] and O-1*s* peak. The observed core-level position is, however, different compared to the Zn-terminated side. On the clean surface the core levels are shifted to ~1 eV lower binding energy compared to the Zn side. The shift in the peak positions is also clearly seen in the valence-band spectra for the two surfaces plotted in Fig. 6. A relative variation in the binding energy of the bulk components between the two surfaces can only be explained by a shift of the Fermi level for the two surfaces since the two samples are electrically connected. With increasing H_2S exposure the peak position for both sides approach the same value [see Fig. 3(a)] indicating that the cause for the shift in the Fermi level is only present for the clean surface. In further variance to the properties of the Zn-terminated side, the O-1*s* peak shows a high binding-energy component that can be assigned to hydroxyls. Figure 7 shows measurements of the O-1*s* peak for

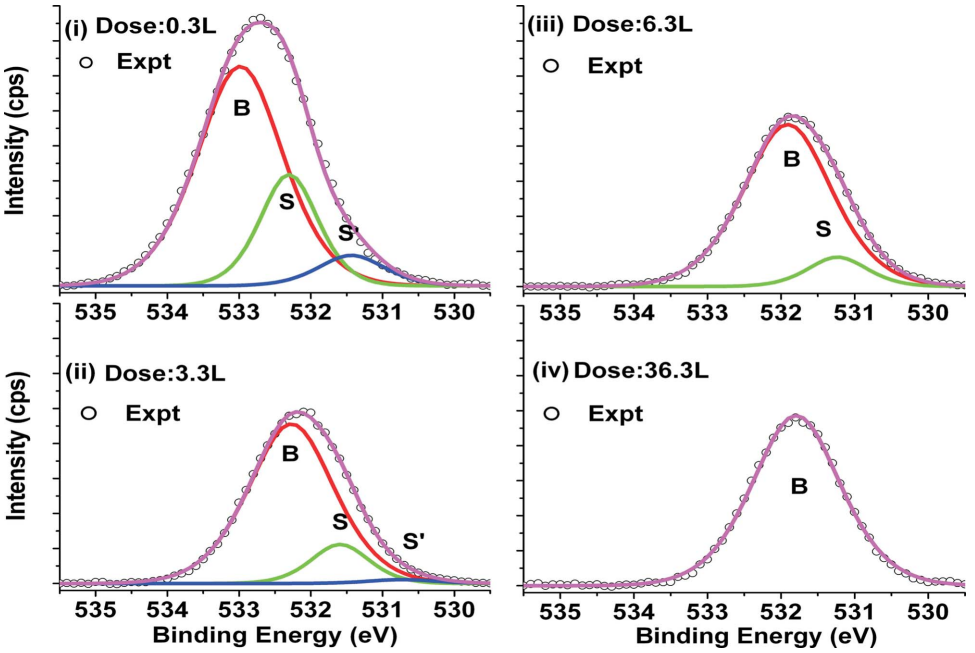

FIG. 4. (Color online) Deconvolution of the O-1*s* core level into bulk (B) and surface (S) components for the ZnO(0001)-Zn surface after H_2S exposure. The surface components S and S′ originate from surface atoms that have different coordination on the terraces (S) and on the steps (S′), respectively, see Fig. 2.

different sample temperatures. This indicates that hydrogen is present at the surface up to ~670 K. Cooling the sample below this temperature results in a rapid reformation of OH. Below 600 K the OH group is increasing due to hydrogen adsorption from the residual gas or hydrogen diffusion from the bulk. The OH peak position for low hydrogen coverage at 600 K and for higher hydrogen coverage does also shift with respect to the main O-1*s* peak. For high OH coverage below 600 K the OH peak is shifted by ~2 eV from the main peak to higher binding energy. This value is consistent with values reported previously.[9] For low coverage at above 600 K the OH peak is shifted by close to 2.5 eV. We speculate that this larger chemical shift for lower OH coverage could have one of two possible origins: (i) the chemical shift is coverage dependent; an assertion based on cluster calculations for core-level positions for ZnO(000–1) that showed

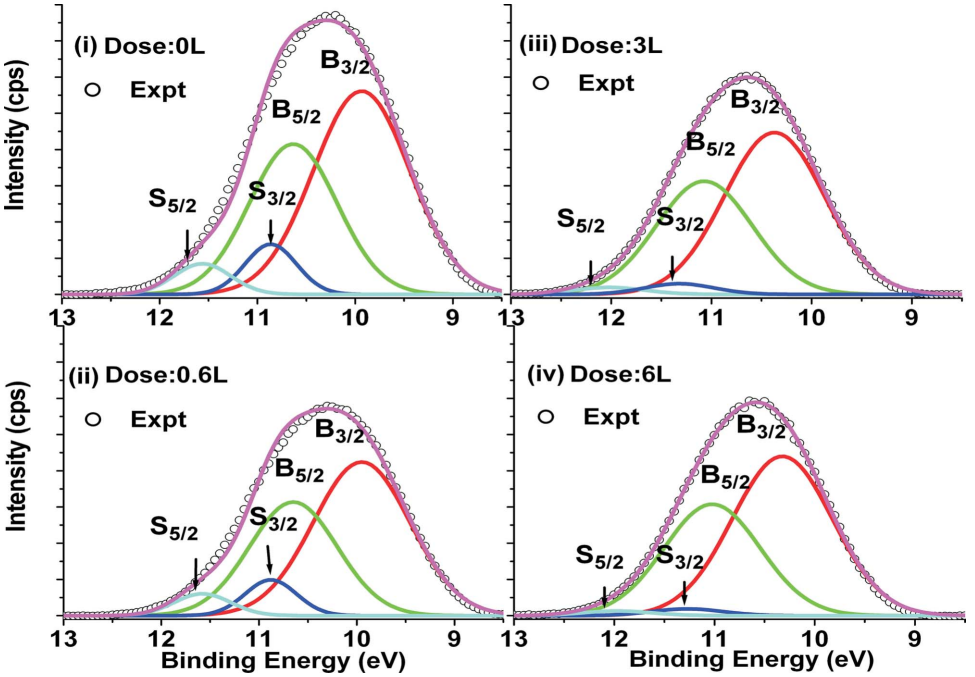

FIG. 5. (Color online) Deconvolution of the Zn-3*d* peak into two spin-orbit doublets, one for the bulk ($B_{3/2}$, $B_{5/2}$) and the surface ($S_{3/2}$, $S_{5/2}$) for the ZnO(0001)-Zn surface before and after H_2S exposure.

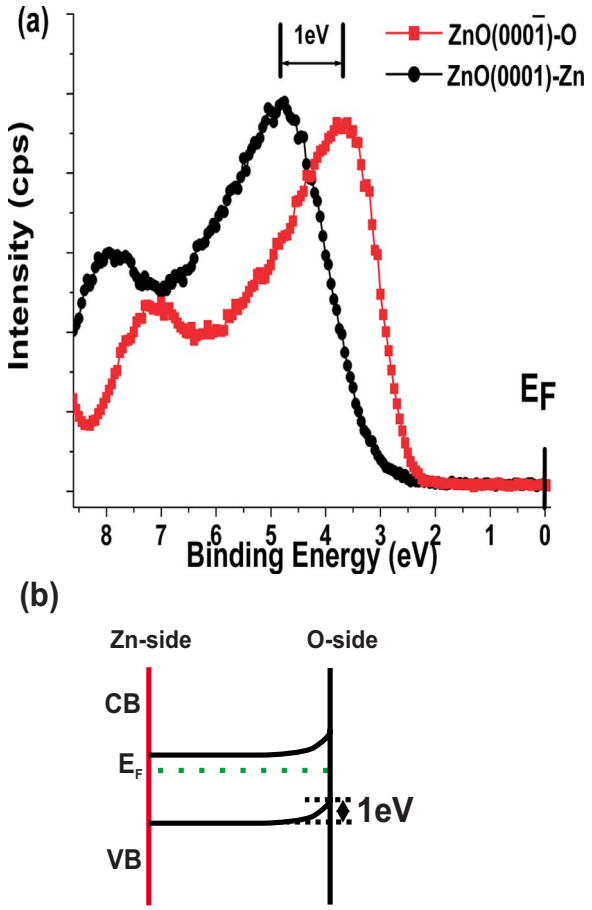

FIG. 6. (Color online) Valence band of the clean ZnO (0001)-Zn and ZnO (000–1)-O surfaces, without H_2S exposure (a). The valence-band maximum is shifted by ~1 eV closer to the Fermi level for the O side compared to the Zn side. This shift in the Fermi level for the two surfaces is illustrated in (b).

significant different O-1*s* positions for 2×1 and 1×1 hydrogen covered surface;[15] or (ii) the high-temperature OH species occupy different sites, e.g., second layer instead of surface. Interestingly, with adsorption of H_2S at 600 K the OH component is disappearing. This can be seen in Figs. 8 and 9, which shows the O-1*s* and Zn-3*d* peaks of the ZnO(000–1)-O for different sulfur concentration.

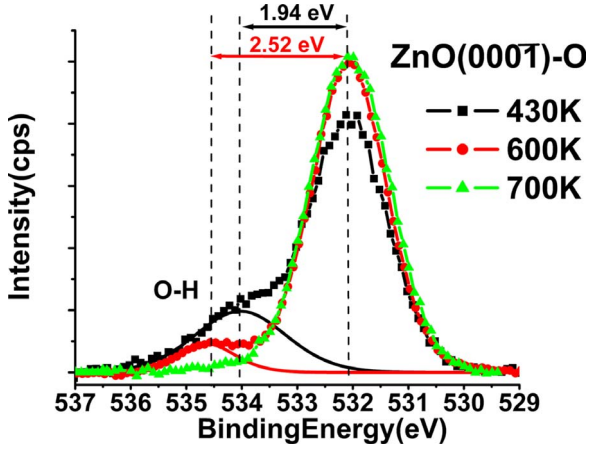

FIG. 7. (Color online) O-1*s* core level acquired at different sample temperature on the ZnO(000–1)-O surface. The shift of the high binding-energy component, assigned to OH is indicated.

IV. PEAK SHAPE ANALYSIS

Peak shapes of semiconducting oxide surfaces are not well described theoretically. To obtain an analytical estimate of the peak shape we fitted the bulk component to a mixed Gaussian/Lorentzian line shape. We obtained a best fit for a 50% Gaussian and 50% Lorentzian for the O-1*s* and 90% Gaussian and 10% Lorentzian for the Zn-3*d* peaks. These line shapes were kept constant throughout the subsequent fitting procedures for the different components. Prior to peak fitting a Shirley background was subtracted to compensate for the secondary electron background.

Two possible origins for the observed peak broadening for the clean surfaces have been considered: (i) Final state effects; i.e., due to the adsorbate induced band bending the surface charge-carrier concentration and consequently the screening of core holes by conduction electrons is affected. This would result in a variation in the screened and unscreened portion of the photoelectron intensity. We show below that this process cannot explain the peak broadening. (ii) Initial state effects; in ionic lattices, surface atoms have a lower Madelung energy relative to the bulk position. This causes a shift of the photoemission line of the surface atoms compared to the bulk. The Madelung energy in a lattice causes a shift of the photoemission line for cations (anions) to lower (higher) binding energy compared to a free ion, this effect is reduced at the surface and consequently a shift of the surface component to higher and lower binding energies relative to the bulk component for cations and anions, respectively, is observed.[16]

First we discuss the possibility of final-state effects. Egdell and co-workers have demonstrated for Sn doped In_2O_3 and Sb doped SnO_2 that final-state effects can contribute significantly to the core-level line shapes.[17,18] These materials are closely related to ZnO because all these materials exhibit a free-electron *s*-like conduction band that gives rise to high conductivity. Because of these similarities one may expect that plasmon losses also could contribute to the observed peak broadening in ZnO. The plasmon loss intensity is expected to scale with $\sqrt[3]{n}$, where n is the charge-carrier concentration, and the plasmon loss energy should be proportional to the $\sqrt{n}$. Since the charge-carrier contribution depends exponentially on the separation between Fermi level and conduction band minimum, a strong variation in charge-carrier concentration is expected for the observed band bending of ~0.5 eV with increasing H_2S exposure for the ZnO(0001)-Zn surface [see Fig. 3(a)]. Thus the band bending enables us to estimate the variation in the charge-carrier concentration n and consequently the expected variation in the intensity and energy position of the screened component. Low amounts of H_2S adsorption resulted already in a large band bending. Consequently, because of an exponential dependence of the charge-carrier concentration, a strong change in the screened component would be expected. Attempts to deconvolute the Zn-3*d* and O-1*s* peaks in a

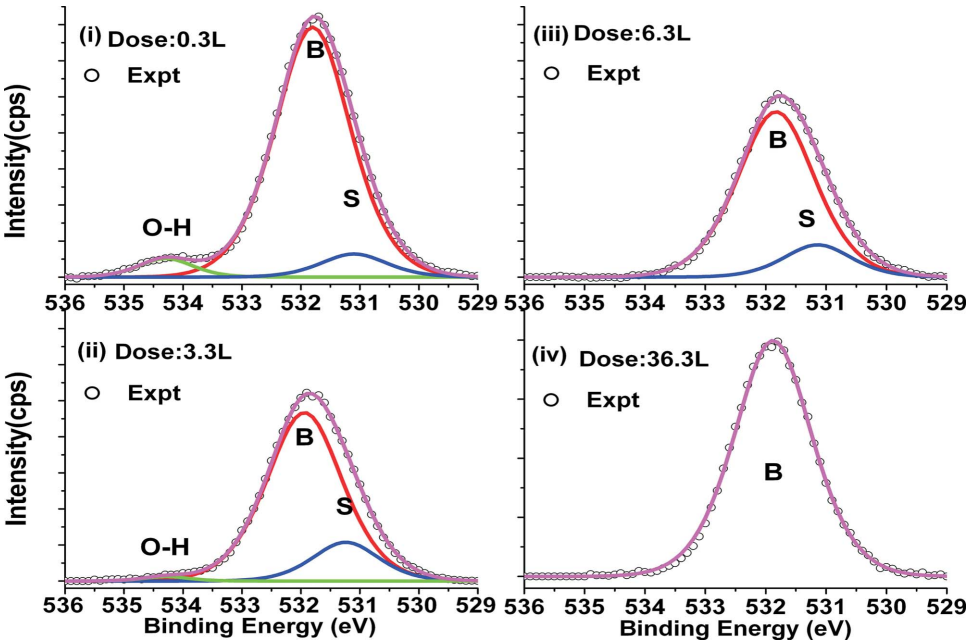

FIG. 8. (Color online) Deconvolution of the O-1*s* peak into bulk (B) and surface (S) components for the ZnO(000–1)-O surface after H_2S exposure.

screened and unscreened components did, however, not satisfy such a strong dependence of the intensity of the screened component on the band bending. This failure of the intensity ratios between screened and unscreened component to reproduce the expected dependence on the amount of band bending already indicates that plasmon losses on these nominally undoped ZnO single crystals do not play a significant role for explaining the peak shape. This conjecture can be made even more convincingly for the ZnO(000–1)-O surface. Here we observe the opposite trend for the Fermi-level position with H_2S exposure, i.e., the Fermi level lies close to the center of the band gap for the clean surface (see below for an explanation for this unexpected observation) and shifts closer to the conduction band with H_2S exposure [see Fig. 3(a)]. Thus stronger plasmon losses would be expected for the sulfur-covered surface compared to the clean surface. This is opposite to the observed larger peak broadening for the clean surface. Consequently we can confidently exclude the possibility that final-state effects contribute significantly to the line shape of undoped ZnO.

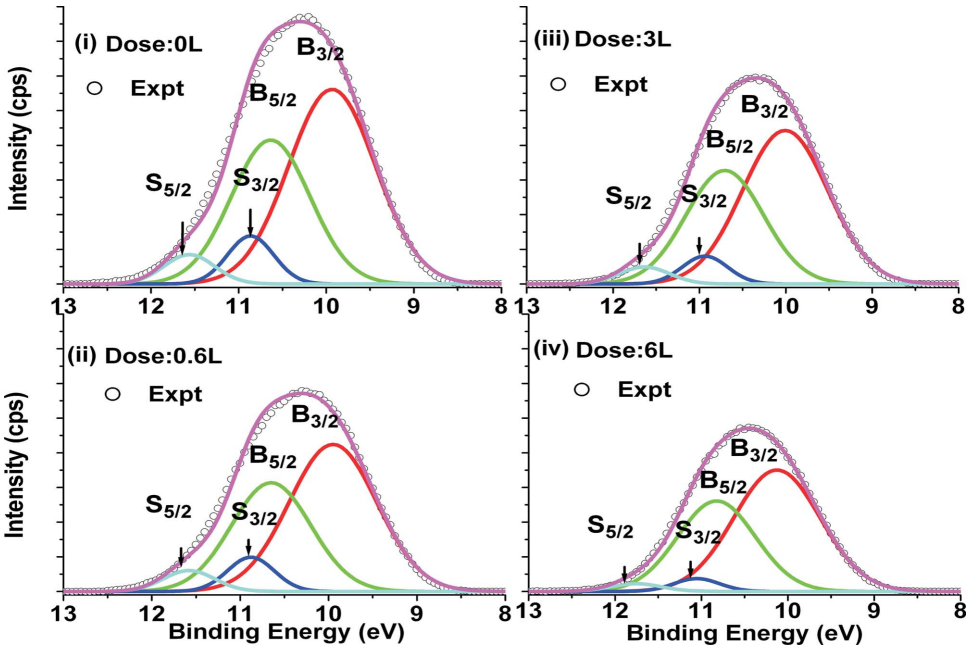

FIG. 9. (Color online) Deconvolution of the Zn-3*d* peak into two spin-orbit doublet, one for the bulk ($B_{3/2}$, $B_{5/2}$) and the surface ($S_{3/2}$, $S_{5/2}$) for the ZnO(000–1)-O surface before and after H_2S exposure.

Now we show that the varying Madelung energies at the surface explain the observed peak broadening for the clean surfaces. Surface effects in core-level photoemission of ionic crystals are well documented for GaAs, ZnSe, and other compound semiconductors.[19,20] Removing the vacuum termination of the substrate by an adsorbate is reducing this surface effect.[21] Consequently, the observed peak narrowing with increased sulfur coverage for both surfaces can be explained by a suppression of the surface component. Sulfur uptake measured from the S-2*p* peak intensity and scanning tunneling microscopy (STM) measurements of sulfidized ZnO surfaces indicate a two-dimensional–layer growth and therefore sulfur is an ideal adsorbate to cover the surface.[14]

The intensity ratio of the surface relative to the bulk component depends on the inelastic mean-free path of the photoemitted electrons. The data shown above were acquired with soft x rays with photon energies of 150 and 630 eV for the Zn-3*d* and O-1*s* peaks, i.e., with kinetic energies of ~125 eV for the photoelectrons. This is the energy range of highest surface sensitivity with a mean-free electron path between 6 and 8 Å, depending on the estimate.[21] A mean-free path of 8 Å translates into an expected surface to bulk ratios of 0.3, for the clean ZnO surfaces. Additional uncertainties may arise due photoelectron diffraction effects. At these low kinetic electron energies elastic backscattered electron may cause interferences that can modulate the photoelectron intensity. From multiple electron-scattering calculations we estimate that this could cause a maximum variation in the surface to bulk ratio of a factor of 2.[22] Nevertheless, the contribution of the surface layer to the photoemission spectrum is considerable and thus the peak broadening could originate from a surface component.[23]

In principle chemical shifts due to sulfur adsorption at the interface between the surface sulfide and the ZnO substrate could also cause a broadening upon surface sulfidation. However, since we observe the opposite trend, i.e., a peak narrowing with increasing sulfide formation, we conclude that chemical shifts due to Zn-S formation are smaller compared to changes in the surface Madelung energy. Thus the observed narrowing is treated solely as a result of removing the surface component and consequently we use the sulfur-covered surface as a measurement of the bulk component of the core-level peaks. This bulk peak shape then enables us to deconvolute the peaks of the clean (or only partially sulfur covered) samples into their bulk and surface components. The results of this peak deconvolution procedure are shown in Figs. 5 and 9 for the two polar surfaces.

The Zn-3*d* peak was not resolved in its 5/2 and 3/2 multiplets. For the fitting procedure these two components were, however, taken into account. The spin-orbit split and the 3/2 to 5/2 peak ratios were constrained to 0.7 eV and a ratio of 2:3, respectively, while the FWHM of the components were kept free. The FWHM of the bulk component was determined from fitting the Zn-3*d* peak at highest sulfur exposure as mentioned above. In subsequent fitting procedure this FWHM value was kept constant. Freely adjustable fitting parameters were the peak positions of the bulk and surface components in order to accommodate band bending. A test for the fitting procedure is that the intensity ratio between the surface and bulk components is expected to decrease for a strictly two-dimensional coverage of the surface by sulfur. Figure 10 shows the intensity ratio of the surface and bulk component of the Zn-3*d* peak as a function of the S-2*p*/Zn-3*d* peak ratio. A monotonous decrease in the surface component is observed for both polar surfaces, indicating a layer growth in agreement with our STM observations.[14]

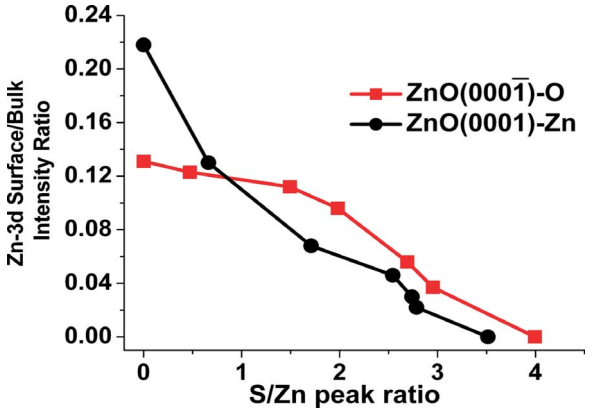

FIG. 10. (Color online) Intensity ratio of the surface component to the bulk component for the Zn-3*d* peak as function of the S or Zn peak ratio.

From the peak deconvolution we observe a shift of the Zn-3*d* surface component of 0.95 eV for the ZnO(0001)-Zn and 0.93 eV for the ZnO(000–1)-O surface relative to the bulk position. This surface shift compares favorable for reported surface components due to the reduced Madelung energy on related materials, such as ZnSe, for which a shift of 0.9 eV has been reported.[20] The deconvolution of the O-1*s* peak followed similar procedures as for the Zn-3*d* peaks. However, it was not always possible to obtain satisfying fits with only two components. For the ZnO(000–1)-O side we have to take the aforementioned hydroxyl oxygen peak into account, while on the ZnO(0001)-Zn side the O-1*s* peak needed to be fit by two lower binding-energy peaks relative to the bulk component. This may indicate the presence of surface oxygen sites with different Madelung energy, i.e., surface sites with different coordination. The intensities of the different peak components (normalized to the full peak area) and the peak positions relative to the bulk components are summarized in Table I for the two surfaces for varying H_2S exposure. It may be also worth mentioning that the observed shifts of the surface components to higher binding energy for the cation (Zn) and lower binding energy for the anion (O) is the expected direction for the surface component due to a reduced Madelung energy at ionic surfaces. Therefore the reduced Madelung energy at the surface causes the observed peak broadening for clean ZnO surfaces.

V. DISCUSSION

The surface structure of the ZnO(0001)-Zn surface prepared in UHV has been thoroughly analyzed by scanning probe techniques.[5,6] These measurements resulted in the conclusion that this polar surface is stabilized by a ~1/4 of a monolayer Zn-deficient surface. This Zn deficiency is estab-

TABLE I. Results of the deconvolution of the surface and the bulk components of the O-1*s* core level for the two polar surfaces for different H_2S exposures. The measured peak-binding energy, full width at half maximum, component intensities normalized to the peak area and the intensity ratio of the surface to bulk component are listed.

Surface	H_2S Dose (L)	Components	BE (eV)	FWHM (eV)	Area	$I(S+S')/I(B)$
ZnO(0001)	0.3	Bulk (B)	552.99	1.41	0.69	0.45
"Zn side"		Surface (S)	552.30	0.95	0.23	
		Step edges (S′)	551.44	1.09	0.07	
	3.3	Bulk (B)	552.27	1.41	0.84	0.18
		Surface (S)	551.59	0.95	0.14	
		Step edges (S′)	550.73	1.09	0.02	
	6.3	Bulk (B)	551.91	1.41	0.89	0.12
		Surface (S)	551.23	0.95	0.11	
	36.3	Bulk (B)	551.80	1.41	1.00	0
ZnO(000–1)	0.3	Bulk (B)	531.82	1.49	0.84	0.19
"O side"		Surface (S)	531.16	1.36	0.11	
		Hydroxyl (OH)	534.28	1.10	0.05	
	3.3	Bulk (B)	531.97	1.49	0.76	0.30
		Surface (S)	531.31	1.36	0.22	
		Hydroxyl (OH)	534.28	0.93	0.01	
	6.3	Bulk (B)	531.85	1.49	0.81	0.23
		Surface (S)	531.85	1.36	0.19	
	36.3	Bulk (B)	531.88	1.50	1.00	0

lished by formation of a high density of step edges that have an O termination, such as shown in Fig. 2. This implies that there are two differently coordinated O sites at the surface. O atoms at step edges have less Zn-cation neighbors, which will result in a larger shift of the Madelung energy relative to terrace and bulk O sites. Consequently, the observed two surface components in the O-1*s* peak for the clean ZnO(0001)-Zn surface is assigned to step and terrace sites. The ratio of the photoelectron intensities of these two peaks of ~0.3 corroborates such an assignment since it is close to the factor of $\frac{1}{4}$ deduced from simple electrostatic stabilization arguments of polar surfaces.[3]

The fact that differently coordinated surface ions have distinctively different Madelung energies and therefore should exhibit different photoemission lines is well established. However, usually surfaces do not exhibit a large number of undercoordinated defect sites. The ZnO(0001)-Zn surface is different than most other surfaces because the stability requirements of this polar surface forces it to create a well defined step edge density. Other surfaces with known step edge densities and structure may, however, be formed by other means, such as formation of vicinal surfaces. In all these cases the differentiation of step edge atoms from terrace sites would enable us to perform site specific studies. For example, adsorption at step edges should be differentiable from adsorption on terrace sites by monitoring the shifted surface components. In our measurements sulfur adsorption causes a more rapid decrease in the surface component assigned to step edges compared to terrace sites. This is consistent with our STM studies that showed that at 600 K that sulfide islands nucleate a step edges but that they form 2D islands thus covering both step edges and terraces.[14]

The stabilization mechanism for the ZnO(000–1)-O polar surface is not well understood. On our samples we always observed OH below sample temperatures of 670 K. The amount of OH increased at lower temperatures. At 600 K the O-1*s* peak intensity associated with hydroxyls did not change significantly with time, suggesting an equilibrium situation. Contamination of the surface with hydrogen lowers the electrostatic energy due to the bulk dipole moments and thus lowers the surface energy. Our observation agrees with previously made assertions that preparation of a hydrogen free ZnO(000–1)-O surface is extremely difficult.[24] At the moment we cannot distinguish if the hydrogen is diffusing out of the bulk (hydrogen is a known bulk impurity in ZnO) or is adsorbed from the residual gas in the UHV chamber.

It is tempting to use the surface sensitivity of soft x-ray photoemission to compare the oxygen and zinc composition of the surface for the two polar surfaces in order to decide if the polar surfaces are stabilized by ion deficiencies. Unfortunately, photoelectron diffraction effects on single-crystal surfaces can influence the measured photoelectron intensity significantly, which makes accurate determination of the surface composition difficult. For instance, using the peak areas normalized by the photon flux, we measure an about 8% more intense Zn-3*d* peak on the ZnO(0001)-Zn side compared to the ZnO(000–1)-O side. This appears to contradict the known stabilization mechanism of the ZnO(0001)-Zn surface by formation of Zn-deficient surface with ~$\frac{1}{4}$ ML Zn missing. Multiple electron-scattering calculations are, however, in agreement with a stronger intensity of surface Zn atoms for the ZnO(0001)-Zn side compared to the ZnO(000–

1)-O surface for the kinetic energies of the photoelectrons used in this study and thus this apparent discrepancy can be explained by diffraction effects. Similar measurements for the O-1*s* signal show an about 3% stronger signal on the O side compared to the Zn side. Although this does not indicate any O deficiency on the O side, photoelectron diffraction effects can offset compositional variations at the surface. Consequently our measurements do not allow an unambiguous determination of the oxygen concentration of the ZnO(000–1)-O surface. More detailed measurements of photoelectron diffraction at different photon energies and emission angles would be necessary to resolve the issue of O composition.

The Fermi-level position for the O and Zn sides is quite different for the two polar surfaces, but approaches the same value for S-covered surfaces [see Fig. 3(a)]. For the Zn-side we measure the valence-band maximum about 3.2 eV below the Fermi edge, i.e., at a position expected for *n*-type ZnO. Thus the Zn-terminated surface does not show any significant variation from the Fermi level position in the bulk. The O side, on the other hand exhibits a shift of the Fermi level by ~1.2 eV closer to the center of the band gap. Such shifts occur due to electrostatic band bending. Electrostatic shifts in binding energies are common for charged molecules adsorbed at the surfaces or formation of interfaces. For the O side the only adsorbate present is hydrogen. Hydrogen, a positively charged adsorbate, always induces a downward band bending (shift of the Fermi level closer to the conduction band), i.e., the opposite from what is observed. Furthermore, a complete removal of hydrogen at 650–700 K as shown in Fig. 7 does not change the position of the Fermi level significantly. Consequently a different mechanism than surface adsorbates is responsible for the Fermi-level shift at the O side.

The obvious explanation comes from the electrostatic potential that builds up at a polar surface if the bulk dipole is not (or only partially) compensated by any other charge-transfer mechanism. This implies that under our experimental conditions there are not enough oxygen vacancies or ionic impurity charges to completely compensate for the electrostatic potential buildup due to the internal dipoles. The downward shift of the Fermi level at the surface in this *n*-type material will result in a positive space-charge region which will contribute to lowering the electrostatic potential at the surface. Our observed Fermi-level shift to about midgap position does not allow for a depletion of valence-band electrons and thus a charge redistribution as described in Fig. 1(b) will not occur. Therefore, unless there exist higher lying surface states that are emptied by pushing the Fermi level to midgap the only charges are from ionized donors that have to exist to make the sample *n* type. However, there are unlikely to be enough donors to provide a large enough positive surface charge (even if it extends over several tens of nanometers into the bulk) to stabilize the surface. Therefore at this point it seems unlikely that the shift of the Fermi level to the midgap is the only stabilization mechanism at elevated temperatures. Nevertheless, our observation is significant since it provides the first experimental evidence that the O side is not completely stabilized by O vacancies or hydrogen at above 600 K. The fact that this shift of the Fermi level is only observed at elevated temperatures, where the hydrogen is desorbed suggests that hydrogen adsorption stabilizes the surface at lower temperatures and possibly is the reason why this shift has not been observed previously. For the Zn side the removal of $\frac{1}{4}$ Zn atoms stabilizes the surface and thus no electrostatic shift of the Fermi level is observed at all temperatures.

It is likely that hydrogen is strongly adsorbed on the ZnO(000–1)-O surface because it stabilizes the polar surface. Thus one may speculate that if a different stabilization mechanism is provided, the hydrogen interaction with the surface is weakened. This hypothesis could explain the following observation: Dissociative adsorption of H_2S provides more hydrogen to the surface, however, as can be seen from the O-1*s* spectra (Fig. 8); the OH shoulder is rapidly decreasing and vanishes completely after exposure of 3.3L H_2S, corresponding to a sulfur coverage of 0.5 ML. Consequently, although there are still plenty of O sites for hydrogen to adsorb, sulfur coadsorption at the surface lowers the desorption temperature of hydrogen. Therefore we propose that for ZnO(000–1)-O hydrogen adsorption is the most likely source for stabilization under regular conditions, but this stabilization mechanism may be influenced by coadsorbates. Consequently coadsorbates may strongly influence the chemical properties of the surface.

VI. CONCLUSIONS

The extreme surface sensitivity of soft x-ray photoemission spectroscopy allowed us a new look on the stabilization mechanisms of the polar ZnO surfaces. The O-1*s* and Zn-3*d* core levels exhibit components that can be assigned to bulk and surface ions. No contributions due to plasmon losses are observed in the core-level spectra. For the ZnO(0001)-Zn surface the stabilization mechanism by formation of Zn vacancies is consistent with the observed peaks. Two surface peaks for O-1*s* are assigned to terrace and step sites. The intensity ratio of these two components is in agreement with $\frac{1}{4}$ ML of surface Zn-atoms missing. The identification of these two different sites may enable the study of site directed surface chemistry in the future. Attenuation of the respective O-1*s* components would enable identification of adsorption at steps or terrace sites. This approach may also have further utility for other oxide surfaces, e.g., vicinal surfaces that exhibit surface sites with different Madelung energy and thus characteristic shifts in the core levels.

For the ZnO(000–1)-O surface we showed that hydrogen is easily adsorbed. At elevated temperature the Fermi level is shifted toward the center of the band gap. This results in depletion of charge carriers in the surface region and thus can contribute to the stabilization of the polar surface. Since the charge-carrier concentration i.e., a positive space-charge region is small in these intrinsically *n*-type doped samples, the shift of the Fermi level alone may not be enough to generate the charge transfer necessary to stabilize the surface. For more highly doped samples the depletion of conduction band electrons may, however, be an effective stabilization mechanism. Such a proposed charge-transfer mechanism may compete with a lowering of the surface en-

ergy by adsorption of hydrogen or other adsorbates and thus would enable a tuning of the chemical surface properties.

ACKNOWLEDGMENTS

The U12a beamline is supported by the Division of Chemical Sciences, Geosciences, and Biosciences, Office of Basic Energy Sciences, U.S. Department of Energy, under Contract No. DE-AC05-00OR22725 with Oak Ridge National Laboratory, managed and operated by UT-Battelle, LLC. Use of the National Synchrotron Light Source, Brookhaven National Laboratory, was supported by the U.S. Department of Energy, Office of Science, Office of Basic Energy Sciences, under Contract No. DE-AC02-98CH10886. Acknowledgment is made to the Donors of the American Chemical Society Petroleum Research Fund for partial support of this research.

[1] P. S. Bagus, F. Illas, G. Pacchioni, and F. Parmigiani, J. Electron Spectrosc. Relat. Phenom. **100**, 215 (1999).
[2] P. W. Tasker, J. Phys. C **12**, 4977 (1979).
[3] C. Noguera, J. Phys.: Condens. Matter **12**, R367 (2000).
[4] J. Goniakowski, F. Finocchi, and C. Noguera, Rep. Prog. Phys. **71**, 016501 (2008).
[5] O. Dulub, L. A. Boatner, and U. Diebold, Surf. Sci. **519**, 201 (2002).
[6] O. Dulub, U. Diebold, and G. Kresse, Phys. Rev. Lett. **90**, 016102 (2003).
[7] M. Kunat, S. G. Girol, T. Becker, U. Burghaus, and C. Wöll, Phys. Rev. B **66**, 081402(R) (2002).
[8] B. Meyer and D. Marx, Phys. Rev. B **67**, 035403 (2003).
[9] C. Wöll, Prog. Surf. Sci. **82**, 55 (2007).
[10] R. Lindsay, C. A. Muryn, E. Michelangeli, and G. Thornton, Surf. Sci. **565**, L283 (2004).
[11] B. Meyer, Phys. Rev. B **69**, 045416 (2004).
[12] R. E. Watson, M. L. Pearlman, and J. W. Davenport, Surf. Sci. **115**, 117 (1982).
[13] E. A. Kraut, R. W. Grant, J. R. Waldrop, and S. P. Kowalczyk, Phys. Rev. B **28**, 1965 (1983).
[14] J. Lahiri and M. Batzill, J. Phys. Chem. C **112**, 4304 (2008).
[15] K. Kotsis and V. Staemmler, Phys. Chem. Chem. Phys. **8**, 1490 (2006).
[16] C. Noguera, F. Finocchi, and J. Goniakowski, J. Phys.: Condens. Matter **16**, S2509 (2004).
[17] R. G. Egdell, T. J. Walker, and G. Beamson, J. Electron Spectrosc. Relat. Phenom. **128**, 59 (2003).
[18] V. Christou, M. Etchells, O. Renault, P. J. Dobson, O. V. Salata, G. Beamson, and R. G. Egdell, J. Appl. Phys. **88**, 5180 (2000).
[19] P. Laukkanen, M. Kuzmin, R. E. Perälä, M. Ahola, S. Mattila, I. J. Väyrynen, J. Sadowski, J. Konttinen, T. Jouhti, C. S. Peng, M. Saarinen, and M. Pessa, Phys. Rev. B **72**, 045321 (2005).
[20] D. A. Evans, D. Wolffframm, D. Gnoth, J. Cairns, A. C. Wright, M. Evans, J. Riley, D. Westwood, and D. A. Woolf, Appl. Surf. Sci. **104-105**, 240 (1996).
[21] W. G. Wilke, V. Hinkel, W. Theis, and K. Horn, Phys. Rev. B **40**, 9824 (1989).
[22] M. Vos, S. G. Anderson, and J. H. Weaver, Phys. Rev. B **39**, 3274 (1989).
[23] F. J. Garcia de Abajo, M. A. Van Hove, and C. S. Fadley, Phys. Rev. B **63**, 075404 (2001).
[24] M. Kunat, U. Burghaus, and C. Wöll, Phys. Chem. Chem. Phys. **5**, 4962 (2003).